The ROYAL COLLEGE of OPHTHALMOLOGISTS

www.nature.com/eye

ARTICLE

Check for updates

A fluorescein angiography-based computer-aided algorithm for assessing the retinal vasculature in diabetic retinopathy

Amir Abbasnejad[1,2], Oren Tomkins-Netzer[3], Aaron Winter[4], Alon Friedman[2,5], Alan Cruess[4], Yonatan Serlin[6] and Jaime Levy[7]✉

OBJECTIVE: To present a fluorescein angiography (FA)–based computer algorithm for quantifying retinal blood flow, perfusion, and permeability, in patients with diabetic retinopathy (DR). Secondary objectives were to quantitatively assess treatment efficacy following panretinal photocoagulation (PRP) and define thresholds for pathology based on a new retinovascular function (RVF) score for quantifying disease severity.

METHODS: FA images of 65 subjects (58 patients and 7 healthy volunteers) were included. Dye intensity kinetics were derived using pixel-wise linear regression as a measure of retinal blood flow, perfusion, and permeability. Maps corresponding to each measure were then generated for each subject and segmented further using an ETDRS grid. Non-parametric statistical analyses were performed between all ETDRS subfields. For 16 patients, the effect of PRP was measured using the same parameters, and an amalgam of RVF was used to create an RVF index. For ten post-treatment patients, the change in FA-derived data was compared to the macular thickness measured using optical coherence tomography.

RESULTS: Compared to healthy controls, patients had significantly lower retinal and regional perfusion and flow, as well as higher retinal permeability ($p < 0.05$). Moreover, retinal flow was inversely correlated with permeability ($R = -0.41$; $p < 0.0001$). PRP significantly reduced retinal permeability ($p < 0.05$). The earliest marker of DR was reduced retinal blood flow, followed by increased permeability. FA-based RVF index was a more sensitive indicator of treatment efficacy than macular thickness.

CONCLUSIONS: Our algorithm can be used to quantify retinovascular function, providing an earlier diagnosis and an objective characterisation of disease state, disease progression, and response to treatment.

Eye (2023) 37:1293–1301; https://doi.org/10.1038/s41433-022-02120-4

INTRODUCTION

Fluorescein angiography (FA) was first introduced more than 50 years ago and remains the "gold standard" for assessing the integrity of the retinal vasculature [1]. Despite its widespread use, however, conventional fundus photography in standard FA evaluates only about 30% of the total retinal area. Recent technological advances now allow the imaging of more than 80% of the retina using a single 200° ultra-widefield FA (UW-FA; Optos, Dunfermline, UK) scan. In addition, the interpretation of FA data is still based on a subjective assessment by the physician and can therefore vary widely [2]. Thus, semi-quantitative methods for measuring retinal perfusion on FA have been developed [3, 4]. For example, retinal blood flow can be measured using the principle of dye dilution tracking, in which the concentration of fluorescein dye within the blood observed at a specific point is plotted against time, producing a dye dilution curve; however, this method is rarely used in clinical practice [5]. In recent years, measuring the area of retinal non-perfusion (RNP) on UW-FA images has gained popularity for studying diabetic retinopathy (DR) and retinal vein occlusion [6–8]. However, the specific methodologies used vary among studies [9], and the non-perfusion area is measured simply in mm^2, with no information regarding retinal vessel permeability. Currently, no quantitative, automated method is available for comparing changes in retinovascular function based on UW-FA data.

We previously described an algorithm developed to quantify retinal vessel permeability using narrow-field FA (NF-FA) [10]. This approach was based on established, validated methods for measuring vascular blood flow and permeability in brain vessels during live imaging in animal models [11].

Here, we present the next-generation algorithm in which we include a quantitative measure of retinal blood flow and perfusion in order to objectively assess various retinovascular functions in patients with proliferative DR. We report that this algorithm can be used to assess both group effects and individual responses to treatment. Finally, we show that this algorithm can be used to functionally assess disease severity.

METHODS

In this retrospective study, we reviewed FA data and medical records from a total of 58 patients with proliferative DR. Thirty-one patients were non-

[1]Faculty of Computer Science, Dalhousie University, Halifax, NS, Canada. [2]Emagix, Inc., Halifax, NS, Canada. [3]Department of Ophthalmology, Faculty of Medicine, Carmel Medical Center, Technion, Haifa, Israel. [4]Department of Ophthalmology, QEII Hospital, Dalhousie University, Halifax, NS, Canada. [5]Departments of Medical Neuroscience and Pediatrics, Faculty of Medicine, Dalhousie University, Halifax, NS, Canada. [6]Neurology Residency Training Program and Department of Neurology and Neurosurgery, Jewish General Hospital (J.M.), McGill University, Montreal, QC, Canada. [7]Department of Ophthalmology, Hadassah-Hebrew University Medical Center, Jerusalem, Israel. ✉email: levjaime@gmail.com

Received: 7 November 2021 Revised: 24 April 2022 Accepted: 20 May 2022
Published online: 28 May 2022

consecutive patients diagnosed and followed at the Retina Clinic, Hadassah Medical Center, Jerusalem, Israel; 15 patients were at Soroka University Medical Center, Beer-Sheva, Israel; and 12 patients were from the Nova Scotia Health Authority, Dalhousie University, Halifax, Canada. All three respective ethics committees approved the study. In addition, we collected data from seven healthy controls from our previous study [10]. Because this study was retrospective, informed consent was not required.

The patients included in our analysis had proliferative DR in either one or both eyes and underwent either NF-FA (Topcon 50EX camera, Ophthalmic Imaging Systems, Sacramento, CA) or UW-FA (Optos, Dunfermline, UK). Pre-treatment and post-treatment data were available for 16 patients who underwent panretinal photocoagulation (PRP). The mean ± SD age at the first UW-FA scan was 54.5 ± 12.8 years; the age at the second NF-FA was 55.4 ± 12.8 years. Among the 58 patients, 39 were male (67%) and 19 were female (33%), and the presenting visual acuity was 0.20 ± 0.50 logMAR. Central retinal thickness measured using optical coherence tomography (OCT) was also available for 10 of the 16 patients treated with PRP and was 333 ± 45 microns.

Images were processed (see Fig. 1) using a custom script in MATLAB (v. 2019b; MathWorks, Natick, MA). Pre-processing included the manual exclusion of any frames that were not suitable for analysis, resulting in the exclusion of 21% of frames due to retinal occlusion, the alternate eye, poor contrast, saturation, overexposure, lack of sharpness, pixelated appearance, and/or inconsistent magnification (see Fig. 1A). In addition, scans from patients with DR who received PRP were manually excluded. Next, the included images were aligned with respect to a reference frame within the set by applying a sequence of rigid transformations using the ORB (Oriented FAST and Rotated BRIEF) [12] feature detector/descriptor (see Fig. 1B). The reference frame was automatically selected from the peak phase with maximum fluorescence in order to provide the largest number of landmarks for the registration process. Timestamps of three frames were selected automatically in order to provide timepoints for analysis as follows: the first critical timepoint, t_1, was the timestamp of the frame approximating the onset of the early arterial phase; the second timepoint, t_2, was the acquisition time of the frame capturing the peak phase (maximal fluorescence); and the third timepoint, t_3, was the acquisition time of the last frame in the test (i.e., the recirculation phase). Within these three timepoints, we performed a pixel-wise analysis of the dynamic changes in signal intensity following the injection of sodium fluorescein in order to map blood flow, permeability, and perfusion, as detailed below (see Fig. 1C). Blood flow maps were generated by calculating the pixel-wise linear regression between timepoints t_1 and t_2 (i.e., the early, rapid increase in intensity following tracer injection). Permeability of the retinal vasculature was estimated by computing the rate of accumulation of the fluorescent dye within the extravascular space using linear regression of the pixels in all frames measured at timepoints t_2 and t_3. Perfusion maps were generated based on the blood flow calculation and were dichotomised by setting a positive flow rate to a value of "1" (perfused); otherwise, the value was set to "0" (non-perfused).

After the map was generated, the Early Treatment Diabetic Retinopathy Study (ETDRS) protocol [13] (ClinicalTrials.gov identifier: NCT00000151) was used to segment the maps into nine regions (Fig. 1D) by manually

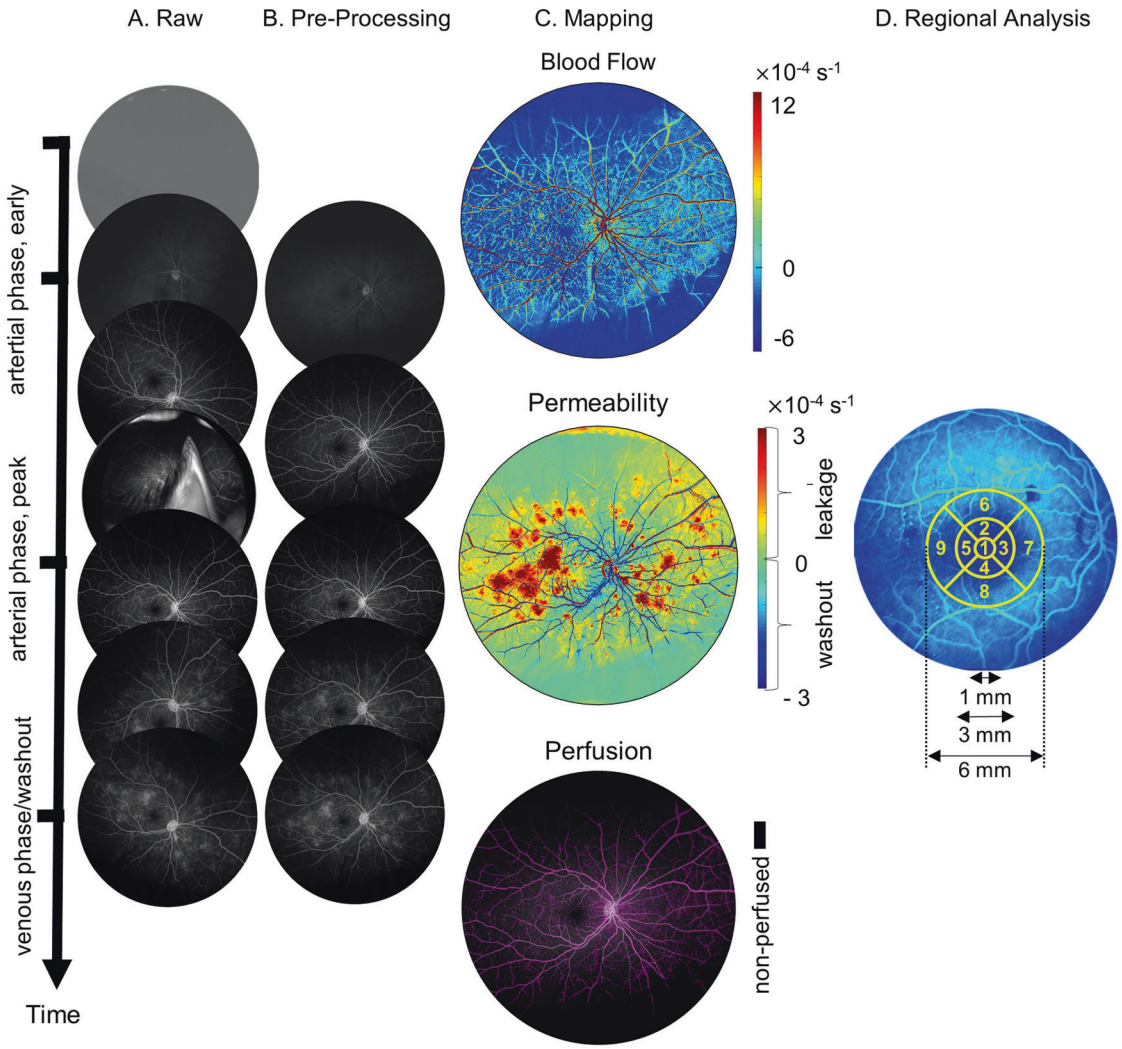

Fig. 1 The approach. A, **B** The original, raw images are pre-processed for the removal of noisy images, and registration. **C** The time series is used to create maps representing blood flow, microvascular permeability, and perfusion. **D** Regional analysis allows for region-wise averaging, with nine regions shown.

determining the width of the optic disc and the location of the fovea. Two-thirds of the optic disc width was assumed to be 1000 microns. The location of the fovea and the scale of the retina were then used to localise the ETDRS subfields. In patients for whom pre-treatment and post-treatment UW-FA scans were available, the ETDRS map was expanded to include a fourth outer concentric circle, which was subdivided into four equal-sized sections (regions 10–13) that were used to capture the periphery of the retina.

Severity was classified by setting thresholds based on the controls in order to produce a binary value of either "0" (for control levels) or "1" (for abnormal or pathological levels). This binary classification was assigned to each of the nine retinal regions. After regional classification, the scores were aggregated per retina to produce a distribution of disease severities; clusters within this resulting distribution were then used to stratify the control and patient retinas into the following four categories: healthy, mild, moderate, and severe. Details regarding the severity classification are provided below.

To determine the threshold for severely impaired blood flow, the flow rate maps were first regionalised into the nine retinal regions. For each region, the flow rate data from healthy controls were then classified into two clusters using a Gaussian mixture model ($k = 2$). In the higher mean cluster (defined here as "healthy" flow rate), values in the 95th percentile were treated as outliers and removed. The threshold for pathological vascular flow was then arbitrarily defined as the bottom 10th percentile of the resulting distribution in each region [14–16]. The cut-off value was set such that <5% of all flow rates measured in the controls would fall below this value. The median regional vascular flow rates measured among the patients were then compared against this threshold to yield a binary score of "1" (for severely impaired; median <10th percentile) or "0" (for otherwise healthy; median ≥10th percentile).

To determine the threshold for abnormal permeability (i.e., "leaky vessels"), we computed two empirical cumulative distribution functions (one for controls and one for patients), as previously reported [10]. The threshold for pathological permeability was defined as any pixel with a permeability value above the 95th percentile of values measured in the controls. The median regional permeability values were then compared against the permeability threshold and assigned a value of "1" (for "pathological"; median >95th percentile) or "0" (for otherwise "healthy"; median ≤95th percentile).

To determine the threshold for reduced perfusion, we again computed two empirical cumulative distribution functions (one for controls and one for patients). The threshold for pathological perfusion was defined as any perfusion in the lower 95th percentile of the control values. Regional perfusion values were compared against the perfusion threshold and assigned a value of "0" (for a pathologically low-perfused region; <95th percentile) or "1" (for otherwise healthy; ≥95th percentile).

We then computed a sum score for each measure (i.e., flow rate, permeability, and perfusion) for each region, yielding a total score per region ranging from 0 to 3 representing disease severity within the region. These nine regional scores were then summed, yielding a final total score ranging from 0 to 27 for the total retina. The total scores were distributed and then manually clustered into the following four categories of disease severity based on the peaks in the distribution of the retinal scores (see Fig. 2C): healthy (total score: 0–4), mild (total score: 5–14), moderate (total score: 15–21), and severe (total score: 22–27).

OCT data were available for 10 of the 16 patients for whom pre- and post-treatment scans were available. Retinal thickness was assigned a score of "1" if >300 microns (for pathological thickness) or "0" if ≤300 microns (for normal thickness) [17]. Regional thickness and index scores were calculated both pre- and post-treatment. The post-treatment scores were then subtracted from the corresponding pre-treatment scores to yield a "Δ thickness" score (see Fig. 3A); similarly, the post-treatment regional index scores were subtracted from the corresponding pre-treatment scores to yield a "Δ index" score (see Fig. 3B).

RESULTS

We first analysed the FA images obtained from 7 healthy controls and 58 patients diagnosed with proliferative DR (Fig. 4). Figure 4A depicts example maps for a patient and a control. Wilcoxon rank-sum tests were used to assess differences in retinal vascular parameters (Fig. 4B, C). Results were considered significant at $p \leq 0.05$. All analyses were performed using Prism version 8.4.3 (GraphPad, USA). We found that compared to controls, the patients had significantly lower retinal blood flow ($p \leq 0.01$), higher permeability ($p \leq 0.05$), and lower perfusion ($p \leq 0.001$) measured both overall (Fig. 4B) and in all 9 retinal regions (Fig. 4C). Moreover, an analysis across all regions revealed lower blood flow ($p \leq 0.001$), higher permeability ($p \leq 0.01$), and lower perfusion ($p \leq 0.001$) in the macula compared to other regions of the retina (data not shown). Across all patients, we also found a significant inverse correlation between permeability and blood flow (Fig. 4D, left) and a significant inverse correlation between permeability and perfusion (Fig. 4D, right); Pearson's correlations were performed using Prism version 8.4.3 (GraphPad, USA).

Sixteen of the patients underwent UW-FA both before and after receiving PRP (Fig. 5). Figure 5A illustrates pre- and post-treatment maps for a single such patient. We found that after PRP, retinal permeability (i.e., vascular leakage) significantly decreased in both the central (R1–R5) and peripheral (R6–R9) regions of the retina, with no significant change in either blood flow or perfusion (Fig. 5B, C; Wilcoxon rank-sum tests). Because the response to treatment varied between patients, we defined a patient as a "responder" if a retinal region showed an increase in blood flow, an increase in perfusion, and/or a decrease in permeability compared to their corresponding pre-treatment UW-FA data (Fig. 5D); we then plotted the percentage of responders based on the change in the central retina and the peripheral retina (Fig. 5D, right panel). We found that approximately 80% and 60% of patients responded with a reduction in central and peripheral permeability, respectively; in addition, approximately 40% and 60% of patients had increased perfusion in the central and peripheral retina, respectively. Finally, approximately 20% of patients had increased blood flow in the central or peripheral retina (Fig. 5D).

Next, we used the control data to establish thresholds for determining pathological values (see Methods and Fig. 2A). These thresholds were then used to dichotomise blood flow, perfusion, and permeability in the 9 regions of the retina. The binary scores were aggregated by region and then summed to obtain a single value for each patient, as shown in Fig. 2B. The distribution of the total scores versus the number of controls and patients revealed four peaks corresponding to a healthy retina, mild disease, moderate disease, and severe disease (Fig. 2C, left). In addition, we sorted the total scores and determined the relative contributions of blood flow, perfusion, and permeability to the total score (Fig. 2C, right). The effect of treatment was also visualised by the change in score for each region (Fig. 2D), showing the heterogeneity among the patients' response to treatment.

Finally, we summarised the post-treatment change in retinal thickness and the regional index scores compared to pre-treatment in all nine regions of the ten patients for which OCT data were available (Fig. 3). We found that the change in the proposed FA-based score in the macula was more sensitive than the change in macular thickness based on the OCT data (Fig. 3).

DISCUSSION

Here, we present a computer algorithm based on FA data for quantifying retinal blood flow, permeability, and perfusion in patients with DR. Comparing patients with DR against healthy controls revealed significant regional differences, which we then used to validate the surrogate measures of retinal blood flow, permeability, and perfusion. As expected in proliferative DR, we found an inverse correlation between retinal blood flow and vascular permeability. An analysis of the effects of PRP in treating patients revealed varied responses and highlights the value of measuring blood flow, permeability, and perfusion in each region of the retina. Interestingly, the majority of treated patients responded with reduced microvascular leakage (i.e., reduced permeability) and increased peripheral perfusion, whereas few patients responded with an increase in blood flow. Combining the measurements into

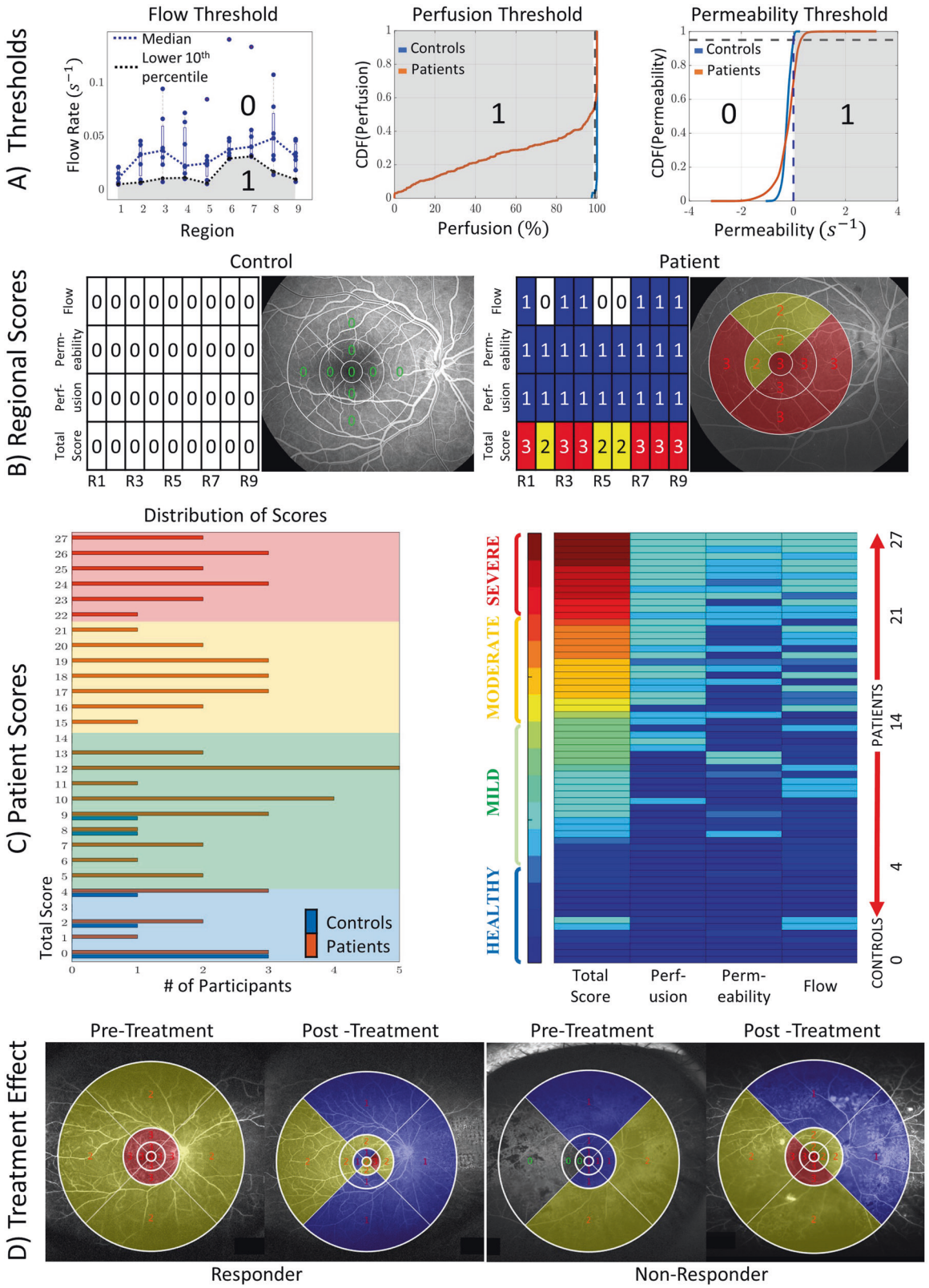

Fig. 2 Using the algorithm to estimate disease severity. A For each parameter, data from the controls and patients were used to define a threshold that was then used to define a value of "0" (healthy) or "1" (pathological). **B** Regional scores for a healthy control (left) and a patient with DR (right) showing the sum scores of pathological findings (ranging from 0–3 for each of the nine regions). **C** Based on the distribution of total scores (ranging from 0–27), disease severity was determined for each patient, ranging from a "healthy" retina to a severely affected retina. **D** A representative severity map in each region is shown for a patient who responded to treatment (left) and a patient whose disease severity worsened or was unchanged after treatment was classified as a non-responder (right).

A

	Δ Retinal Thickness								
	R1	R2	R3	R4	R5	R6	R7	R8	R9
1	0	0	0	0	0	0	0	0	0
2	0	0	0	0	0	0	0	0	0
4	0	0	0	0	0	0	0	-1	-1
5	0	0	0	1	0	1	0	0	0
6	-1	-1	-1	-1	-1	-1	-1	-1	-1
7	0	0	0	0	0	0	0	0	0
8	0	0	0	0	0	0	0	0	0
9	0	0	0	0	0	0	0	0	0
10	1	0	0	0	0	0	0	0	1

B

	Δ Index Score								
	R1	R2	R3	R4	R5	R6	R7	R8	R9
1	1	1	2	1	0	1	1	1	2
2	0	-1	0	0	-1	0	0	0	0
4	1	0	1	2	2	1	1	2	2
5	-1	-1	0	-1	-1	-1	-1	-2	-1
6	1	0	-1	0	1	0	0	0	-1
7	-2	-1	-1	-1	-1	1	0	1	1
8	1	2	1	2	1	2	2	2	2
9	0	0	0	0	0	0	1	0	0
10	-1	-1	-1	0	-1	-1	-2	0	-1

Legend

Improved | No Change | Worsened

Fig. 3 Effect of PRP on retinal thickness versus the estimated disease severity. A Regional retinal thickness was defined as either "1" (pathological, >300 µm) or "0" (healthy, ≤300 µm), and regional differences between pre-treatment and post-treatment classification were calculated in ten patients. **B** Regional index scores were calculated for the same patients in **A** using the hierarchical classification scheme described in the Methods (see also Fig. 2). Note that the majority of patients had no change in retinal thickness ("0") but did show a change in index scores.

an aggregate index via a hierarchical thresholding scheme shows the value of combining these three measures in order to stratify disease severity and characterise the patient's response. Interestingly, we found that a change in blood flow was the earliest measurable change in our patients, followed by an increase in permeability. Finally, regional comparisons of these index scores against retinal thickness show that this approach can be useful for characterising treatment efficacy.

DR is often characterised by a progressive decrease in retinal perfusion accompanied by an increase in areas of irreversible RNP [18]. These changes in the retinal vasculature reflect a dynamic process that determines the rate of vision loss. Our algorithm provides an automated, quantitative assessment of the functional dynamics of the fluorescent signal both in the vessels (for measuring blood flow) and in the extravascular space (for assessing vascular leakage). We found that compared to healthy controls, the patients with DR had significantly lower retinal blood flow, higher permeability, and lower perfusion. Moreover, we found that treatment with PRP—without including anti-vascular endothelial growth factor (anti-VEGF) therapy—was effective at reducing vascular permeability in the retina, including the central retina, when assessed 11 ± 8.5 months after treatment. Importantly, however, the effect of PRP varied among patients, as PRP reduced vascular permeability in the majority of patients, while its effects on blood flow and vascular perfusion varied among patients. Finally, our scoring system that combines all three parameters suggests that decreased retinal blood flow is the earliest observable change in DR, followed by an increase in microvascular permeability and decreased perfusion (i.e., retinal ischaemia) in more advanced cases.

In recent years, the ability to quantitatively measure haemodynamic parameters has shown promise with respect to detecting, monitoring, and assessing treatment efficacy in various retinopathies. Several such techniques have been developed, with their respective strengths and weaknesses discussed comprehensively in published reviews [19]. Despite progress, some methods provide haemodynamic parameters that can be difficult to interpret, leading to contradictory results regarding the same disease measured under otherwise similar conditions [19]. In addition, in previous studies researchers manually measured changes in the retinal vasculature, for example by exporting the images to a processing programme such as ImageJ (National Institutes of Health, Bethesda, MD) and then delineating the areas of RNP in a binary fashion ("yes" or "no"), thus introducing subjectivity and potential error, while limiting replicability.

An important finding of our study is the presence of population-level differences in the FA-derived functional parameters, as illustrated in Fig. 4. The negative correlations between vessel permeability and blood flow and between vessel permeability and perfusion are consistent with the pathophysiology of DR, in which increased retinovascular permeability (i.e., leakage) causes local oedema and/or the constriction of retinal capillaries, resulting in retinal ischaemia. Ischaemia in turn leads to the production of various growth factors such as VEGF [20], which stimulates the growth of new, leaky vessels. In this respect, the sensitivity of our approach to detecting this pathophysiological phenomenon is noteworthy.

OCT-angiography (OCTA) has become a widely accepted clinical imaging modality for quantitatively assessing haemodynamics, with several studies suggesting that OCTA can more accurately delineate areas of RNP areas compared to non-quantitative FA [21]. However, OCTA has limitations, the most notable of which is that it cannot be used to quantify vascular leakage or blood flow [22]; moreover, OCTA has a higher risk of acquisition artefacts.

Thus, FA remains an important diagnostic tool for detecting vascular leakage. Notably, we found that the most robust effect of PRP was to reduce vascular permeability. Moreover, the areas of non-perfusion visible on OCTA can represent capillary occlusion, capillary dropout (i.e., a complete loss of capillaries), or impaired perfusion (i.e., extremely slow—or completely absent—blood flow within the existing retinal capillaries), which cannot be differentiated [23]. In contrast, FA can clearly show the retinal microvasculature and blood flow dynamics. Furthermore, the limited ability of OCTA to assess the retinal periphery limits its relevance with respect to diagnosing some early retinopathies. On the other hand, UW-FA can visualise approximately three-fold more total retinal area compared to standard 7-field (ETDRS 7SF) imaging [24]. Indeed, several studies found that UW-FA showed more severe DR due to the visibility of additional peripheral lesions in areas that were beyond the view of ETDRS 7SF imaging [24–26]. These and other findings led to the recent cross-sectional study by the Diabetic Retinopathy Clinical Research Retina Network, protocol AA [27], in which they investigated the role of UW-FA in identifying non-perfusion, neovascularization, and other pathological changes in DR, as well as determining the clinical relevance of peripheral retinal findings in retinopathy outcome.

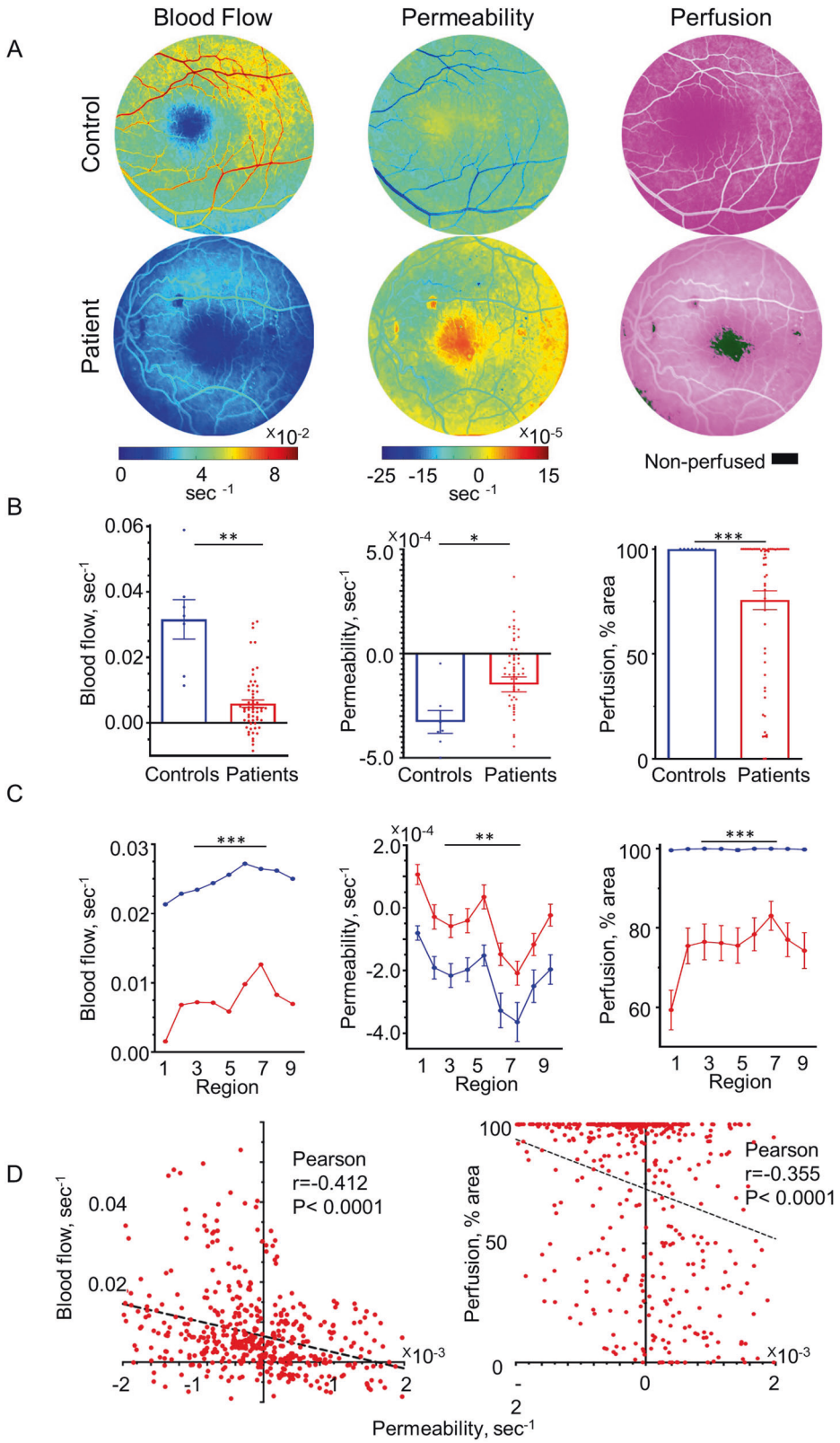

Fig. 4 Summary of retinal vascular parameters measured in healthy controls and patients with diabetic retinopathy. A Representative maps showing blood flow, permeability, and perfusion in a healthy control (top row) and in a patient with DR (bottom row). **B** Summary of the change (SEM) in blood flow, permeability, and perfusion measured in controls ($N = 7$) and patients with DR ($N = 58$). **C** The changes in blood flow, permeability, and perfusion are shown for healthy controls and patients measured in each region of the retina. *$p \leq 0.05$, **$p \leq 0.01$, and ***$p \leq 0.001$ (Wilcoxon rank-sum test). **D** The change in blood flow (left) and the change in perfusion (right) are plotted against the change in permeability for each pixel (Pearson's correlations shown).

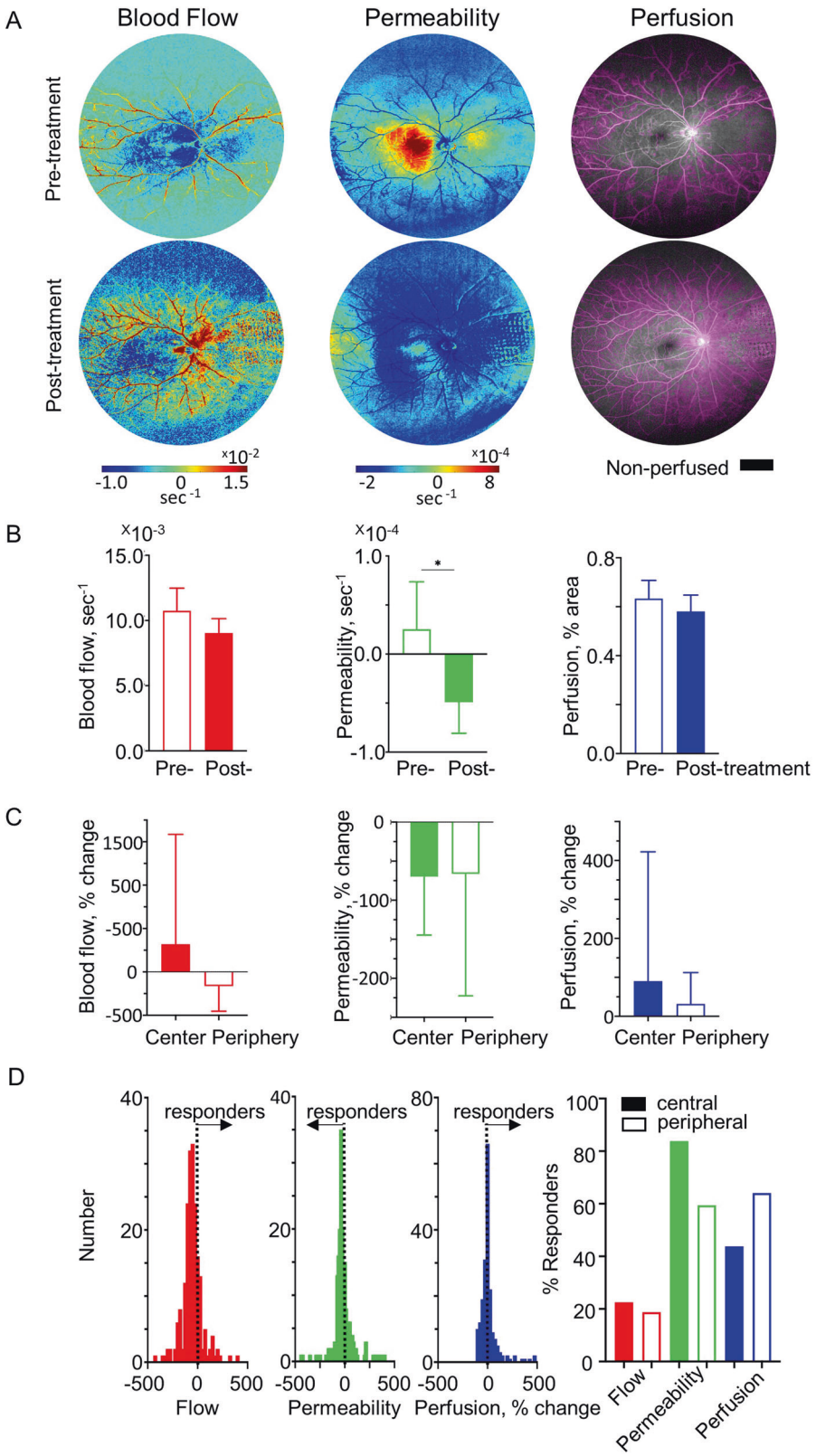

Fig. 5 Assessment of the effect of panretinal photocoagulation (PRP) in patients with DR. In 16 patients, FA was performed both before and after PRP. **A** Representative maps showing the blood flow, permeability, and perfusion in a patient with DR measured before (top row) and after (bottom row) treatment (with SEM bars). **B** Whole-retinal average pre-treatment and post-treatment changes in blood flow, permeability, and perfusion. *$p \leq 0.05$ (Wilcoxon rank-sum test). **C** Summary of the per cent change in blood flow, permeability, and perfusion between the pre-treatment and post-treatment measures in the central retina (regions 1–5) and peripheral retina (regions 10–13). **D** Distributions (left) and summary (right) of the percentage of patients who responded in the central and peripheral regions of the retina.

Currently, no consensus has been reached regarding differences in efficacy between PRP and various anti-VEGF therapies [22]. This lack of consensus is due in part to discrepancies in the literature with respect to the effects of PRP and intravitreal anti-VEGF injections on retinal perfusion. Earlier studies based on laser Doppler velocimetry suggested that PRP reduces retinal blood flow and decreases venous diameter in patients with DR [28–30]. However, recent studies using widefield OCTA suggest that retinal perfusion does not change significantly following PRP in patients with DR [31]. While some studies suggest that intravitreal injections of anti-VEGF may slow the progression of RNP and improve retinal perfusion [18, 32], other studies provide evidence that anti-VEGF injections are unlikely to improve retinal perfusion and may not prevent the gradual progression of non-perfusion or the loss of the peripheral visual field commonly associated with worsening DR [22]. In addition, after stopping anti-VEGF therapy, substantial vision loss may occur if recurrent neovascularization leads to serious ocular complications such as vitreous haemorrhage, retinal detachment, and/or neovascular glaucoma.

The major outcome for determining treatment efficacy in DR is the long-term (i.e., at least 1 year) change in visual acuity. However, this measure is far from perfect, as a patient with neovascularization can have 20/20 (6/6) vision and no warning signs of visual impairment [33]. In these patients, substantial vision loss can occur as these new vessels—and the resulting surrounding contractile fibrous tissue—grow and cause either a vitreous haemorrhage or a tractional retinal detachment. Thus, the algorithm described in this study may provide a more rapid, quantitative, objective, and regionalised assessment of retinovascular function and treatment response, as illustrated in Fig. 2, in which the retinal parameters are amalgamated in order to stratify disease severity. Interestingly, and as mentioned above, this approach shows that reduced flow is the earliest evidence of disease, followed by increased permeability. Ischaemia (i.e., reduced perfusion) is evident in later stages of the disease, thus offering insights into the pathogenesis and progression of DR. In a subset of our patient cohort, we also found that following PRP, changes in retinal thickness measured on OCT were evident in only 20% of patients, compared to changes in retinal vascular function measured in 70% of patients, suggesting that the FA-based algorithm may be more sensitive for following patients after treatment. When using widefield OCTAs, even in clinical trials, as much as 30–40% of scans are of poor quality, as opposed to widefield FAs [34, 35]. In clinical practice, these numbers should be higher so we cannot presently rely on widefield OCTA to replace widefield FA. However, future studies should explore the value of future OCT/OCTA-derived metrics such as a retinal and choroidal change in thickness and vessel calibre in assessing vascular functions and outcomes with respect to visual acuity.

Limitations of our study include the retrospective collection of data and the relatively small number of healthy controls and patients with DR, particularly patients with mild disease. In addition, although combining FA data collected from three different centres and using different cameras shows that the method is likely not equipment-specific or protocol-specific, we cannot rule out the possibility that differences in data acquisition may have affected the signal-to-noise ratio and/or the quality of fit to the models (e.g., linear regression).

On the other hand, a strength of our approach is that it can be used for the rapid, automatic generation of quantitative, regionalised metrics that can then be used to objectively assess DR and can be amalgamated in order to gain insights into the various stages of the disease. Our findings, therefore, support the notion that this algorithm can be used to detect early changes in the retinal vasculature, determine disease severity, and follow disease progression and treatment efficacy.

CONCLUSIONS

Our algorithm can be used to quantify retinal vascular blood flow, permeability, and perfusion, providing an objective, sensitive, and quantitative measure of retinal microvascular function. Future studies should include larger patient cohorts and additional retinal pathologies, thus providing information regarding the role of this approach in diagnosis, treatment efficacy, and follow-up. In this respect, a successful measure of retinovascular function may be more sensitive than structural imaging in providing an early diagnosis of pathogenic changes in the microvascular pathology.

Summary

What was known before

- Fluorescein angiography (FA) remains the “gold standard” for assessing the retinal vasculature.
- Interpretation of FA data is still based on a subjective assessment by the physician and can therefore vary widely.

What this study adds

- The reported algorithm can be used to quantify retinal vascular blood flow, permeability, and perfusion.
- It provides an objective, sensitive, and quantitative measure of retinal microvascular function.

DATA AVAILABILITY

The datasets generated during and/or analysed during the current study are available from the corresponding author on reasonable request.

REFERENCES

1. Flocks M, Miller J, Chao P. Retinal circulation time with the aid of fundus cinephotography. Am J Ophthalmol. 1959;48:3–10.
2. Friedman SM, Margo CE. Choroidal neovascular membranes: reproducibility of angiographic interpretation. Am J Ophthalmol. 2000;130:839–41.
3. Bertram B, Wolf S, Fiehöfer S, Schulte K, Arend O, Reim M. Retinal circulation times in diabetes mellitus type 1. Br J Ophthalmol. 1991;75:462–5.
4. Tomic L, Mäepea O, Sperber GO, Alm A. Comparison of retinal transit times and retinal blood flow: a study in monkeys. Invest Ophthalmol Vis Sci. 2001;42:752–5.
5. Or C, Sabrosa AS, Sorour O, Arya M, Waheed N. Use of OCTA, FA, and ultra-widefield imaging in quantifying retinal ischemia: a review. Asia-Pac J Ophthalmol. 2018;7:46–51.
6. Tan CS, Li KZ, Sadda SR. Wide-field angiography in retinal vein occlusions. Int J Retin Vitreous. 2019;5:18.
7. Fan W, Uji A, Wang K, Falavarjani KG, Wykoff CC, Brown DM, et al. Severity of diabetic macular edema correlates with retinal vascular bed area on ultra-wide field fluorescein angiography: DAVE study. Retina. 2000;40:1029–37.
8. Yu G, Aaberg MT, Patel TP, Iyengar RS, Powell C, Tran A, et al. Quantification of retinal nonperfusion and neovascularization with ultrawidefield fluorescein angiography in patients with diabetes and associated characteristics of advanced disease. JAMA Ophthalmol. 2020;138:680–8.
9. Tan CS, Chew MC, van Hemert J, Singer MA, Bell D, Sadda SR. Measuring the precise area of peripheral retinal non-perfusion using ultra-widefield imaging and its correlation with the ischaemic index. Br J Ophthalmol. 2016;100:235–9.
10. Serlin Y, Tal G, Chassidim Y, Parmet Y, Tomkins O, Knyazer B, et al. Novel fluorescein angiography-based computer-aided algorithm for assessment of retinal vessel permeability. PLoS One. 2013;8:e61599.
11. Prager O, Chassidim Y, Klein C, Levi H, Shelef I, Friedman A. Dynamic in vivo imaging of cerebral blood flow and blood-brain barrier permeability. Neuroimage. 2010;49:337–44.
12. Rublee E, Rabaud V, Konolige K, Bradski G. ORB: an efficient alternative to SIFT or SURF. Abstracts of the 2011 International Conference on Computer Vision. Barcelona, Spain: 2011. p. 2564–71.
13. Early Treatment Diabetic Retinopathy Study Research Group. Classification of diabetic retinopathy from fluorescein angiograms. Ophthalmology. 1991;98:807–22.

14. Schoknecht K, Prager O, Vazana U, Kamintsky L, Harhausen D, Zille M, et al. Monitoring stroke progression: In vivo imaging of cortical perfusion, blood-brain barrier permeability and cellular damage in the rat photothrombosis model. J Cereb Blood Flow Metab. 2014;34:1791–801.
15. Yu Y, Han Q, Ding X, Chen Q, Ye K, Zhang S, et al. Defining core and penumbra in ischemic stroke: a voxel- and volume-based analysis of whole brain CT perfusion. Sci Rep. 2006;6:1–7.
16. Bivard A, Levi C, Krishnamurthy V, Hislop-Jambrich J, Salazar P, Jackson B, et al. Defining acute ischemic stroke tissue pathophysiology with whole brain CT perfusion. J Neuroradiol. 2014;41:307–15.
17. Brown JC, Solomon SD, Bressler SB, Schachat AP, DiBernardo C, Bressler NM. Detection of diabetic foveal edema: contact lens biomicroscopy compared with optical coherence tomography. Arch Ophthalmol. 2004;122:330–5.
18. Levin AM, Rusu I, Orlin A, Gupta MP, Coombs P, D'Amico DJ, et al. Retinal reperfusion in diabetic retinopathy following treatment with anti-VEGF intravitreal injections. Clin Ophthalmol. 2017;11:193–200.
19. Pournaras CJ, Riva CE. Retinal blood flow evaluation. Ophthalmologica. 2013;229:61–74.
20. Aiello LP. Angiogenic pathways in diabetic retinopathy. N Engl J Med. 2005;353:839–41.
21. Couturier A, Rey P-A, Erginay A, Lavia C, Bonnin S, Dupas B, et al. Widefield OCT-angiography and fluorescein angiography assessments of nonperfusion in diabetic retinopathy and edema treated with anti-vascular endothelial growth factor. Ophthalmology. 2019;126:1685–94.
22. Jampol LM, Glassman AR, Sun J. Evaluation and care of patients with diabetic retinopathy. N Engl J Med. 2020;382:1629–37.
23. Jia Y, Bailey ST, Hwang TS, McClintic SM, Gao SS, Pennesi ME, et al. Quantitative optical coherence tomography angiography of vascular abnormalities in the living human eye. Proc Natl Acad Sci USA. 2015;112:E2395–402.
24. Wessel MM, Aaker GD, Parlitsis G, Cho M, D'Amico DJ, Kiss S. Ultra-wide-field angiography improves the detection and classification of diabetic retinopathy. Retina. 2012;32:785–91.
25. Silva PS, Cavallerano JD, Haddad NMN, Kwak H, Dyer KH, Omar AF, et al. Peripheral lesions identified on ultrawide field imaging predict increased risk of diabetic retinopathy progression over 4 years. Ophthalmology. 2015;122:949–56.
26. Talks SJ, Manjunath V, Steel DHW, Peto T, Taylor R. New vessels detected on widefield imaging compared to twofield and sevenfield imaging: Implications for diabetic retinopathy screening image analysis. Br J Ophthalmol. 2015;99:1606–9.
27. Aiello LP, Odia I, Glassman AR, Melia M, Jampol LM, Bressler NM, et al. Comparison of Early Treatment Diabetic Retinopathy Study standard 7-field imaging with ultrawide-field imaging for determining severity of diabetic retinopathy. JAMA Ophthalmol. 2019;137:65–73.
28. Grunwald JE, Riva CE, Sinclair SH, Brucker AJ, Petrig BL. Laser doppler velocimetry study of retinal circulation in diabetes mellitus. Arch Ophthalmol. 1986;104:991–6.
29. Grunwald JE, Brucker AJ, Petrig BL, Riva CE. Retinal blood flow regulation and the clinical response to panretinal photocoagulation in proliferative diabetic retinopathy. Ophthalmology. 1989;96:1518–22.
30. Grunwald JE, Brucker AJ, Grunwald SE, Riva CE. Retinal hemodynamics in proliferative diabetic retinopathy. A laser doppler velocimetry study. Invest Ophthalmol Vis Sci. 1993;34:66–71.
31. Russell JF, Al-Khersan H, Shi Y, Scott NL, Hinkle JW, Fan KC, et al. Retinal nonperfusion in proliferative diabetic retinopathy before and after panretinal photocoagulation assessed by widefield OCT angiography. Am J Ophthalmol. 2020;213:177–85.
32. Wykoff CC, Shah C, Dhoot D, Coleman HR, Thompson D, Du W, et al. Longitudinal retinal perfusion status in eyes with diabetic macular edema receiving intravitreal aflibercept or laser in VISTA study. Ophthalmology. 2019;126:1171–80.
33. Bressler NM, Beck RW, Ferris FL. Panretinal photocoagulation for proliferative diabetic retinopathy. N Engl J Med. 2011;365:1520–6.
34. Tan B, Chua J, Lin E, Cheng J, Gan A, Yao X, et al. Quantitative microvascular analysis with wide-field optical coherence tomography angiography in eyes with diabetic retinopathy. JAMA Netw Open. 2020;3:1–13.
35. Lujan BJ, Calhoun CT, Glassman AR, Googe JM, Jampol LM, Melia M, et al. Optical coherence tomography angiography quality across three multicenter clinical studies of diabetic retinopathy. Transl Vis Sci Technol. 2021;10:1–10.

AUTHOR CONTRIBUTIONS

The authors' responsibilities were as follows: AF and JL formulated the research question and designed the study; AW, AC, YS and JL obtained data; AA analysed the data; AA, OT-N, AL, YS and JL: interpreted the findings and wrote the article. All authors read and approved the final manuscript.

COMPETING INTERESTS

AA and AF: Emagix, Inc., Halifax, Nova Scotia, Canada. The other authors declare no competing interests.

ADDITIONAL INFORMATION

Correspondence and requests for materials should be addressed to Jaime Levy.

Reprints and permission information is available at http://www.nature.com/reprints

Publisher's note Springer Nature remains neutral with regard to jurisdictional claims in published maps and institutional affiliations.